Novel Rate Constants for a Catalytic Hydrogenation Reaction of Propylene Obtained by a Frequency Response Method

Yusuke Yasuda,* Kayo Iwai, and Kazumi Takakura

Faculty of Science, Toyama University, Toyama 930, Japan

Received: March 15, 1995; In Final Form: September 18, 1995[⊗]

"Reaction rate (or FR) spectra" of a catalytic hydrogenation of propylene over Pt or Rh at 314 K were observed in a cell reactor composed of a proton-conducting membrane. It is shown that a variety of the spectra can be reproduced well by "characteristic functions", $K^*_H(\omega)$ and $K^*_C(\omega)$, which may be derived from a three-stage model composed of five elementary steps: $X(g) \rightleftharpoons A_X(a) \rightleftharpoons B_X(a) \rightarrow$ propane (X: hydrogen or propylene), where X denotes the gaseous molecule; A_X and B_X are the first and second intermediate adsorbed species. Seven rate constants concerning these five steps were evaluated by matching $K^*_H(\omega)$ or $K^*_C(\omega)$ to the spectrum; five of them, k_{PX}, k_{-AX}, k_{AX}, k_{-BX}, and k_{BX}, are ordinary rate constants, while the other two, l_{-BX} and l_{BX}, are novel ones. Since all these constants except k_{PX} are independent of the amounts of catalyst, they are characteristic of active sites and can be compared with each other. On the basis of these constants, kinetic details have been discussed; for instance, mean residence times of A_X and B_X, τ_{AX} and τ_{BX}, respectively, were determined by $(k_{-AX} + k_{AX})^{-1}$ and $(k_{-BX} + k_{BX})^{-1}$, resulting in (in second units) $\tau_{AH} \sim 0.3$ and $\tau_{BH} \sim 3$ for hydrogen and $\tau_{AC} \sim 3$ and $\tau_{BC} \sim 3$ for propylene over Pt, while over Rh they were $\tau_{AH} \sim 1$ and $\tau_{BH} \sim 3$; $\tau_{AC} \sim 10^2$ and $\tau_{BC} \sim 10^2$. The nondimensional rate constants, l_{-BX} and l_{BX}, were indispensable to reproduce the various FR spectra; l_{-BH} and l_{BH} were positive, whereas l_{-BC} and l_{BC} were negative over both catalysts, which suggests heat effects.

1. Introduction

Periodic perturbation or frequency response (FR) methods have widely been applied to study various relaxation phenomena;[1] for example, chemical relaxation phenomena associated with inter- and intramolecular proton transfer reactions have been investigated by ultrasonic techniques.[2] However, most of them were limited to a homogeneous system.

A rate spectrum characteristic of a *gas/surface* dynamic phenomenon can be obtained by the present FR method. Analogous to a spectroscopic method, this relatively new method is powerful to investigate separately various rate processes occurring simultaneously and to create a basis for quantitative description of the kinetic phenomena.[3] The first application of the FR method to a reactive system at a steady state was performed with a catalytic hydrogenation of propylene over Pt/Al_2O_3 at 273 K.[4] It was found that an unusual rate equation expressed by $R(P_H,\dot{P}_H)$ was effective to interpret the rate spectra with respect to propylene ($C_3{}^{2-}$) and propane (C_3), where R denotes the appearance rate of C_3 or the disappearance rate of $C_3{}^{2-}$, P_H is the partial pressure of H_2, and $\dot{P}_H$ denotes the time derivative, dP_H/dt. It should be emphasized that the novel rate equation involving $\dot{P}$, $R(P,\dot{P})$, has never been required to reproduce theoretically a rate spectrum obtained in a nonreactive system by the FR method.[3] Further, it has never been needed by any traditional methods. Therefore, it would be challenging work to study the nature of the new variable $\dot{P}$.

The originality of this work consists of three main points.

(1) Although a mixture of the reactants has usually been contacted with catalysts in standard methods, as shown in Figure 1a, the reactants are separated by a proton-conducting membrane in this work, as shown in Figure 1b, on both sides of which catalysts are deposited, so that the competitive rate processes of the dissociation of H_2 into 2H (I) and the association of 2H to an olefin C^{2-} (II) could be separately investigated.

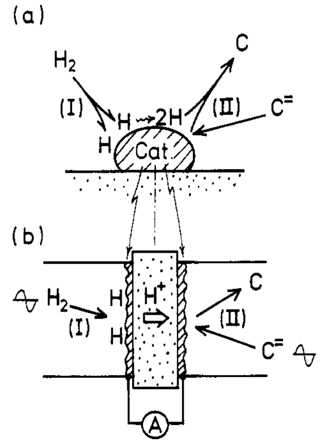

Figure 1. Basic idea of the present FR method. (a) In a usual reactor, a mixture of the two reactants, H_2 and an olefin (C^{2-}), is admitted and the (competitive) two rate processes, the dissociation (I) and association (II) of H_2, producing alkane (C), occur simultaneously. (b) The two rate processes, I and II, are separated in this work by a proton-conducting membrane. The migration of atomic hydrogen on catalysts can be detected by current due to the flow of H^+ across the membrane. If pressure of either H_2 or C^{2-} is varied harmonically, the current would also be varied harmonically and its amplitude and phase lag would depend on the frequency. On the basis of these FR data, kinetic details of the two rate processes could be separately investigated.

(2) The surface migration of atomic hydrogen on catalysts could be detected by the current of H^+ across the membrane.

(3) Let the pressure of either H_2 or C^{2-} be forced to oscillate harmonically by varying the volume of a reactor (using complex notation):

$$P(t) = \bar{P} + \Delta P(t); \quad \Delta P(t) = \Delta P \exp(i\omega t) \qquad (1)$$

where $\bar{P}$ denotes the mean pressure corresponding to that at a steady state of the reaction (see Figure 1b) and ω is the angular frequency. Then the current of H^+, I, would also be oscillated,

---

[⊗] Abstract published in *Advance ACS Abstracts*, December 1, 1995.

0022-3654/95/2099-17852$09.00/0

and the variation induced may be expressed in general by

$$\Delta I(t) = \Delta I_\omega \exp\{i(\omega t - \phi)\} \qquad (2)$$

Since we shall usually choose a condition of $\Delta P/\bar{P} \ll 1$, the variation can be expressed as

$$\Delta I(t) = K^{*}_{\rm obs}(\omega)\, \Delta P(t) \qquad (3)$$

where

$$K^{*}_{\rm obs}(\omega) = \frac{\Delta I_\omega}{\Delta P} \exp(-i\phi) \qquad (4)$$

The coefficient $K^{*}_{\rm obs}(\omega)$ may be observed and is named a "reaction rate (or FR) spectrum".

On the other hand, "characteristic functions", $K^{*}_{\rm H}(\omega)$ and $K^{*}_{\rm C}(\omega)$, have been derived on the basis of a Horiuti–Polanyi mechanism to interpret $K^{*}_{\rm obs}(\omega)$. A variety of FR spectra are shown to be reproduced well by these functions.

2. Experimental Section

2.1. Membrane Catalyst. A proton-conducting membrane (Nafion 117; DuPont) was used as solid polymer electrolyte; platinum or rhodium catalysts were deposited on both sides of the membrane by a chemical plating method by Takenaka and Torikai.[5] The apparent densities of Pt and Rh were ca. 1 × 10 mg/cm^2.

2.2. Apparatus. The FR apparatus is schematically shown in Figure 2a, and the detailed structure of the pyrolytic graphite electrodes to support the membrane is depicted in Figure 2b. The system was sealed with greaseless stopcocks and a sheet of Viton.

Since the conductance of the membrane was ca. 0.1 Ω^{-1} when it was exposed to wet H_2 (~20 Torr; 1 Torr = 133.32 Pa), it may be regarded as a proton conductor. The temperature of the membrane was kept at 314 K; since the humidity of the membrane decreases with increasing temperature, there was an optimum temperature around 314 K.

Hydrogen (in commercial cylinder; 99.99% pure) and propylene (in commercial cylinder; 99.8% pure) were used without further purification.

2.3. Current of H$^+$. The current of H^+ across the membrane was controlled by means of a potentiometric method; the electric circuit outside of the cell reactor is shown in Figure 3. The protonic current I_C can be determined by measuring E_A and E_C:

$$I_C = \frac{10^3}{10^3 - R_C}\left(\frac{E_A}{10^3} - \frac{E_C}{R_C}\right) \qquad (5)$$

where R_C denotes the resistance of a variable resistor of 1 kΩ; E_A (or E_C) is the potential difference between A (or C) and O.

Let us introduce the short notation $H_2|Pt//Pt|C_3{}^{2-}$, which means that gaseous H_2 and C_3H_6 ($C_3{}^{2-}$) were admitted into the compartments separated by the membrane on both sides of which Pt was deposited; in this work, the other system denoted by $H_2|Rh//Rh|C_3{}^{2-}$ was also investigated for comparison.

Typical data on I_C (determined by eq 5) are shown versus E_C in Figure 4a,b which were observed in a $H_2|Pt//Pt|C_3{}^{2-}$ system; dependence on the pressure of either $H_2(P_H)$ or $C_3{}^{2-}(P_C)$ is demonstrated. Obviously, the dependence on P_H was greater than that on P_C. In the measurements, only R_C was changed (although electrodes of the battery were exchanged to make $E_A < 0$ for the measurements over the range of $E_C < 0$); E_A remained almost constant, and therefore the internal resistance of the battery E_A can be neglected. Since the proton cannot be supplied by $C_3{}^{2-}$, the membrane behaved like a diode.

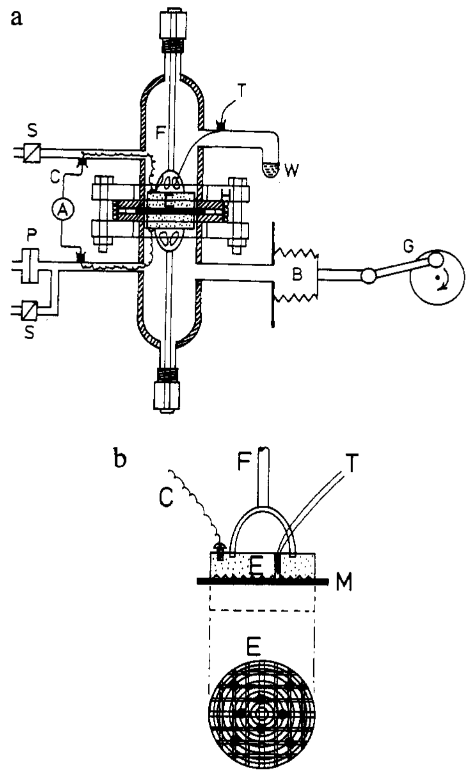

Figure 2. Schematic representation of the FR apparatus. (a) Cell reactor: (A) electric circuit to determine the protonic current, detail of which is shown in Figure 3; (B) metal bellows to vary the gas space; (C) leading wire; (E) electrodes made of pyrolytic graphite; (F) holder made of glass to fix the electrode; (G) sinusoidal wave generator; (H) coil heater to keep the temperature of membrane constant; (P) pressure gauge (MKS Baratron, type 223BD); (S) greaseless stopcock using O-rings; (T) thermocouple; (W) distilled water at room temperature to keep moisture in the gas constant in order to wet the membrane. (b) Detailed structure of the pyrolytic graphite electrodes (37 mm diameter): (C) leading wire; (E) electrode to collect electrons, on the contact surface of which V-shaped grooves and holes were made to make the diffusion of the gas to the membrane easier; (M) Nafion-H, on both sides of which Pt or Rh was deposited.

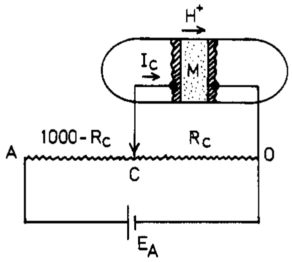

Figure 3. Electric circuit to supply voltage to control and determine the current of H^+, I_C, across the membrane by a potentiometric method: (M) membrane; (R_C) resistance of a variable resistor of 1 kΩ; (E_A) a battery.

The activity of catalysts only slowly decreased (week by week).

2.4. FR Measurements. The gas space of the lower compartment (= ca. 1 dm^3, see Figure 2a) was varied sinusoidally by means of metal bellows after a steady state was attained. The pressure variation induced was expressed well by eq 1; the mean value of the oscillation $\bar{P}$ was usually 20 Torr in this work; and the amplitude ΔP was rather small, i.e.,

$$\Delta P/\bar{P} \approx 0.06 \qquad (6)$$

Changes in the I_C–E_C curve when the pressure of H_2 or $C_3{}^{2-}$ was increased or decreased are schematically shown by the three

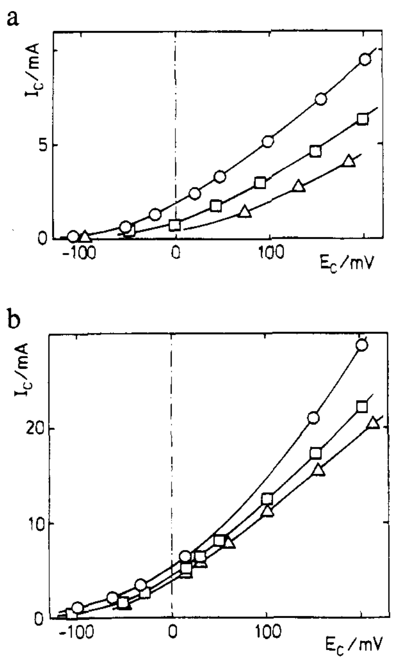

Figure 4. Typical data on I_C versus supplied voltage E_C at 314 K obtained in a system of $H_2|Pt//Pt|C_3^{2-}$. (a) Dependence on the pressure of hydrogen: P_H/Torr = 10 (△), 20 (□), and 40 (○), while P_C was kept at 20 Torr. (b) Dependence on the pressure of propylene: P_C/Torr = 10 (△), 20 (□), and 40 (○), while P_H was kept at 20 Torr.

lines in Figure 5; each conductance κ of the three lines given by the slope may be regarded as identical because of the small amplitude of the oscillation. On the other hand, since I_C and E_C are always correlated with each other by eq 5, the change induced by the pressure variation occurs along the dashed straight line in Figure 5, which is given by

$$\Delta I_C(t) = -\frac{10^3}{(10^3 - R_C)R_C}\Delta E_C(t) \qquad (7)$$

The variation $\Delta I_C(t)$ was determined by measuring $\Delta E_C(t)$ by a pen recorder. However, we are interested in $\Delta I(t)$ indicated by the broad arrow along the vertical line in Figure 5. One easily finds that $\Delta I(t)$ can be determined by adding two terms:

$$\Delta I(t) = \left\{\frac{10^3}{(10^3 - R_C)R_C} + \kappa\right\}\{-\Delta E_C(t)\} \qquad (8)$$

Consequently, the FR spectrum $K^*_{obs}(\omega)$ defined by eq 4 may be determined by

$$K^*_{obs}(\omega) = \left\{\frac{10^3}{(10^3 - R_C)R_C} + \kappa\right\}(\Delta E_\omega/\Delta P)\exp(-i\phi)$$

$$\equiv (\Delta I_\omega/\Delta P)\exp(-i\phi) \qquad (9)$$

where ΔE_ω denotes the amplitude of ΔE_C and ϕ is the phase difference between $-\Delta E_C(t)$ and $\Delta P(t)$; R_C was around 10 Ω and κ was around $3 \times 10^{-2}\ \Omega^{-1}$ in this work; ω was scanned over a range from 0.002 to 0.5 Hz.

Change in $\bar{P}_H$ was negligible in the course of the FR measurements.

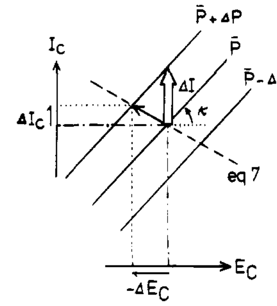

Figure 5. Change in the current of H^+ induced by ΔP_H or ΔP_C during FR measurements. ΔI_C was determined by measuring ΔE_C. However, we are interested in ΔI (see text).

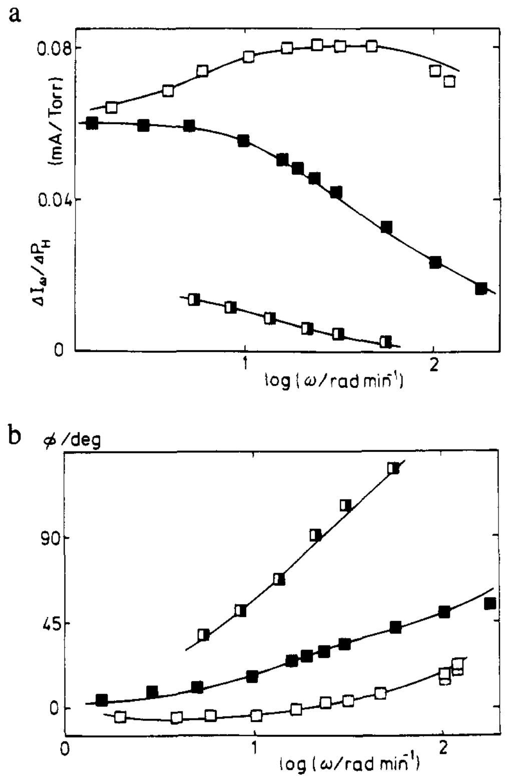

Figure 6. FR data to ΔP_H obtained in three different systems: (□) in $\tilde{H}_2|Pt//Pt|C_3^{2-}$, (■) in $\tilde{H}_2|Pt'//Pt'|C_3^{2-}$, and (◨) in $\tilde{H}_2|Rh//Rh|C_3^{2-}$; the tilde of $\tilde{H}_2$ means that the pressure of hydrogen P_H was varied. (a) The relative amplitude $\Delta I_\omega/\Delta P_H$ versus ω. (b) The phase lag of ϕ versus ω. Each solid curve represents calculated results from $K^*_H(\omega)$ with the seven parameters given in Table 2 corresponding to small circles in Figure 8a.

3. Results

(1) First, let us consider FR data obtained in a $\tilde{H}_2|Pt//Pt|C_3^{2-}$ system; the tilde of $\tilde{H}_2$ means that P_H was varied. The relative amplitude $\Delta I_\omega/\Delta P_H$ and phase lag ϕ are plotted versus ω by open symbols in parts a and b of Figure 6, respectively; other data obtained in a separate series carried out with a different Pt membrane, denoted by $\tilde{H}_2|Pt'//Pt'|C_3^{2-}$, are plotted together by solid symbols.

(2) On the other hand, FR data obtained in the $H_2|Pt//Pt|\tilde{C}_3^{2-}$ and $H_2|Pt'//Pt'|\tilde{C}_3^{2-}$ systems are plotted by open and solid symbols in Figures 7a,b; the tilde of $\tilde{C}_3^{2-}$ means that P_C was varied in this case.

(3) FR data obtained in another series of measurements with Rh catalysts, $\tilde{H}_2|Rh//Rh|C_3^{2-}$ and $H_2|Rh//Rh|\tilde{C}_3^{2-}$, are plotted by the half-solid symbols in Figures 6 and 7 for comparison.

Every two kinds of data, $\Delta I_\omega/\Delta P_X$ and phase lag ϕ, are plotted simultaneously by a vector, as shown in Figure 8a,b; an example for the transformation is demonstrated by the arrow.

4. Theoretical Section

4.1. Reaction Mechanism. A variety of papers about catalytic hydrogenation reactions of light olefins have been

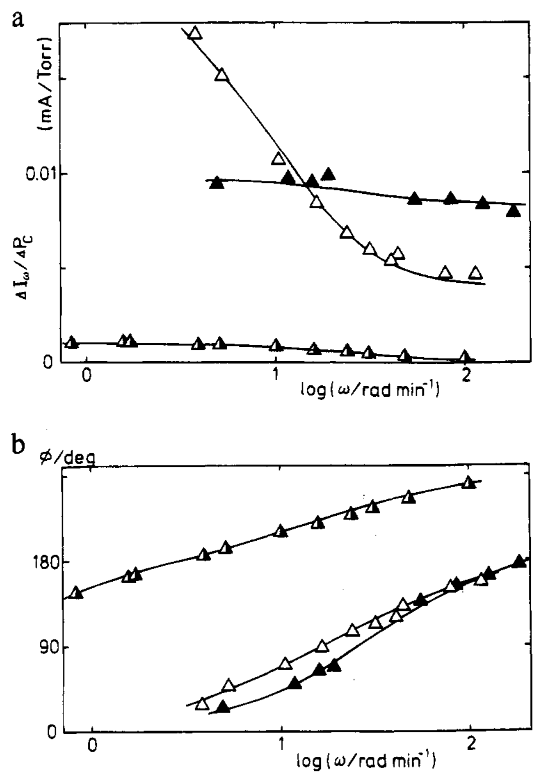

Figure 7. FR data to ΔP_C obtained in three different systems: (△) in $H_2|Pt//Pt|C_3^{2-}$, (▲) in $H_2|Pt'//Pt'|\tilde{C}_3^{2-}$, and (▲) in $H_2|Rh//Rh|\tilde{C}_3^{2-}$; the tilde of $\tilde{C}_3^{2-}$ means that the pressure of propylene P_C was varied. (a) The relative amplitude $\Delta I_\omega/\Delta P_C$ versus ω. (b) The phase lag of ϕ versus ω. Each solid curve represents calculated results from $K_C^*(\omega)$ with the seven parameters given in Table 2 corresponding to the small circles in Figure 8b.

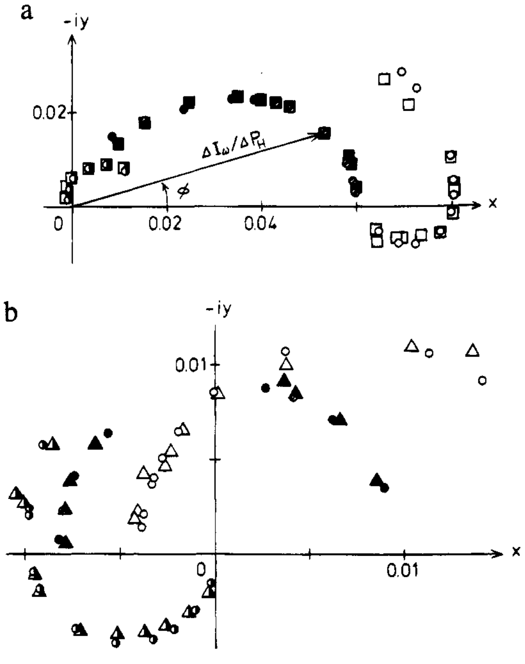

Figure 8. Comparison of FR data with calculated results. (a) Polar plots of the FR data on $\Delta I_\omega/\Delta P_H$ and ϕ given in Figure 6a,b. An example for the transformation is demonstrated by the arrow. (b) Polar plots of the FR data on $\Delta I_\omega/\Delta P_C$ and ϕ given in Figure 7a,b. Each circle represents calculated results from $K_H^*(\omega)$ or $K_C^*(\omega)$ using the seven parameters summarized in Table 2. The notation is that of Figure 6 or 7.

published, and the Horiuti–Polanyi mechanism,[6] containing half-hydrogenated adsorbed species (see Figure 9), has widely been supported.[7,8] Recently, on the basis of steady-state kinetic

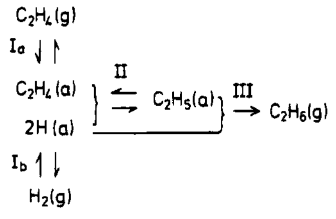

Figure 9. Horiuti–Polanyi mechanism for catalytic hydrogenation of ethylene.

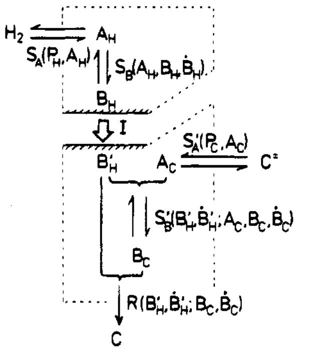

Figure 10. Rate equations contained in the three-stage model, of which variables are explicitly shown. Characteristic functions, $K_H^*(\omega)$ and $K_C^*(\omega)$, have been derived from these functions on the basis of material balance only. The protonic current in Figure 1b is indicated by I.

studies, deuterium tracing measurements, vibrational spectroscopy, and temperature-programmed desorption, a Horiuti–Polanyi mechanism modified by a hydrogen activation step has been proposed.[9]

Based on the mechanism, a three-stage model containing five elementary steps,

$$X(g) \overset{S_A}{\rightleftharpoons} A_X(a) \overset{S_B}{\rightleftharpoons} B_X(a) \overset{R}{\rightarrow} \text{product (X: H or C)}$$

is adopted in this work, where X represents H_2 or olefins in the gas phase; A_X and B_X denote the first and second intermediate adsorbed species, respectively; and the subscript H or C indicates hydrogen or olefins, respectively.

4.2. Rate Equation at Each Stage. Rate equations at the three stages are demonstrated in Figure 10. The basic assumptions for them are as follows.

(1) S_A and S'_A at the First Stage. According to Langmuir kinetics, the rate equation at the first stage may be described by (subscript X is omitted for simplicity)

$$dA/dt = k_aP(N_s - A)^n - k_dA^n, \quad n = 1 \text{ or } 2 \qquad (10)$$

where A denotes the amount of adsorbed species A; P is the pressure of adsorbate; k_a and k_d are the rate constants for adsorption and desorption, respectively; and N_s is the amount of sites available for the adsorption.

It is assumed therefore that the rate equation for the adsorption–desorption of H_2 or olefins at the first stage can be described in general by a function of both P and A:

$$S_A = S_A(P_H,A_H) \qquad (11)$$

and

$$S'_A = S'_A(P_C,A_C) \qquad (12)$$

where P_H and P_C denote the pressures of H_2 and the olefin, respectively; A_H and A_C are the amounts of adsorbed species produced at the first stage.

(2) S_B at the Second Stage of H_2. The second stage for H_2 corresponds to the hydrogen activation;[9] S_B would be affected by both A_H and B_H, where B_H denotes the amount of atomic hydrogen produced at the second stage. Let us introduce a working hypothesis here: only variable B is accompanied by the other variable $\dot{B}$ ($\equiv dB/dt$), so that we have

$$S_B = S_B(A_H,B_H,\dot{B}_H) \tag{13}$$

This hypothesis is based on the fact that the unusual rate equation of $R(P,\dot{P})$ was effective in reactive systems, as reported previously.[4,10,11] It should be emphasized that this function does not exclude any ordinary rate equation expressed by $S_B(A_H,B_H)$.

(3) S'_B at the Second Stage of Olefins. The second stage for olefins corresponds to the initial hydrogenation (or transformation of A_C to B_C); S'_B would be affected by B'_H, A_C, and B_C, where B'_H denotes the amount of atomic hydrogen located on the opposite side of the membrane (see Figure 10). According to the hypothesis, we have

$$S'_B = S'_B(B'_H,\dot{B}'_H;A_C,B_C,\dot{B}_C) \tag{14}$$

(4) R at the Third Stage. Since the last stage would be affected by B'_H and B_C, considering the hypothesis, we have

$$R = R(B'_H,\dot{B}'_H;B_C,\dot{B}_C) \tag{15}$$

(5) It is assumed further that B'_H is proportional to B_H, which means no phase lag between B'_H and B_H; it would be accepted when the membrane is a proton conductor:

$$B'_H(t) = gB_H(t) \ (g\text{: constant}) \tag{16}$$

4.3. Characteristic Functions. On the basis of the various rate equations demonstrated in Figure 10, we can derive two kinds of characteristic functions to describe FR spectra as follows.

When the pressure of a reactant is varied, the amount of A and then that of B would also be varied. Their variations may be expressed in general by

$$A(t) = \bar{A} + \Delta A_\omega \exp\{i(\omega t - \psi_A)\} \equiv \bar{A} + \Delta A^*_\omega \exp(i\omega t) \tag{17}$$

and

$$B(t) = \bar{B} + \Delta B_\omega \exp\{i(\omega t - \psi_B)\} \equiv \bar{B} + \Delta B^*_\omega \exp(i\omega t) \tag{18}$$

provided that $\Delta P(t)/\bar{P} \ll 1$, where ΔA_ω and ΔB_ω denote the amplitudes of the oscillation and ψ_A and ψ_B are the phase lags behind the pressure variation (the subscript X for A and B is omitted for simplicity).

Since the variation was harmonic, we evidently have

$$\dot{B}(t) = i\omega \Delta B^*_\omega \exp(i\omega t) \tag{19}$$

Substituting eq 1 and eqs 17−19 into the various rate equations in Figure 10, we can derive variations in all elementary reaction rates, ΔS_A, $\Delta S'_A$, ΔS_B, $\Delta S'_B$, and ΔR, induced by $\Delta P(t)$. In the derivation, the Taylor series expansion to the first order, i.e.,

$$f(x+\Delta x,y+\Delta y) = f(x,y) + (\partial f/\partial x)_y \Delta x + (\partial f/\partial y)_x \Delta y \tag{20}$$

was available irrespective of the functional form, because the relative amplitude of the volume variation and necessarily that of the pressure variation was small. Consequently, all rate equations can be linearized.

TABLE 1: Seven Rate Constants Involved in Each Characteristic Function, $K^*_H(\omega)$ or $K^*_C(\omega)$

	$S_A(P_H,A_H)$	$S_B(A_H,B_H,\dot{B}_H)$	$S'_B(B'_H,\dot{B}'_H;A_C,B_C,\dot{B}_C) +$ $R(B'_H,\dot{B}'_H;B_C,\dot{B}_C)$
$K^*_H(\omega)^a$	$(\partial S_A/\partial P_H)_A \equiv k_{PH}$ $-(\partial S_A/\partial A_H)_P \equiv k_{-AH}$	$(\partial S_B/\partial A_H)_B \equiv k_{AH}$ $-(\partial S_B/\partial B_H)_A \equiv k_{-BH}$ $-(\partial S_B/\partial \dot{B}_H)_A \equiv l_{-BH}$	$[\partial(S'_B + R)/\partial B_H] \equiv k_{BH}$ $[\partial(S'_B + R)/\partial \dot{B}_H] \equiv l_{BH}$
	$S'_A(P_C,A_C)$	$S'_B(B'_H,\dot{B}'_H;A_C,B_C,\dot{B}_C)$	$R(B'_H,\dot{B}'_H;B_C,\dot{B}_C)$
$K^*_C(\omega)^b$	$(\partial S'_A/\partial P_C)_A \equiv k_{PC}$ $-(\partial S'_A/\partial A_C)_P \equiv k_{-AC}$	$(\partial S'_B/\partial A_C)_B \equiv k_{AC}$ $-(\partial S'_B/\partial B_C)_A \equiv k_{-BC}$ $-(\partial S'_B/\partial \dot{B}_C)_A \equiv l_{-BC}$	$(\partial R/\partial B_C) \equiv k_{BC}$ $(\partial R/\partial \dot{B}_C) \equiv l_{BC}$

[a] For a $\tilde{H}_2|//|C^{2-}$ system. [b] For a $H_2|//|\tilde{C}^{2-}$ system.

(1) In a $\tilde{H}_2//C^{2-}$ Case. Let us consider a case where P_H is perturbed. On the basis of material balance, the appearance rate of A_H species can be expressed by

$$dA_H/dt = S_A(P_H,A_H) - S_B(A_H,B_H,\dot{B}_H) \tag{21}$$

and that of B_H species is given by

$$dB_H/dt = S_B(A_H,B_H,\dot{B}_H) - S'_B(B'_H,\dot{B}'_H;A_C,B_C,\dot{B}_C) - R(B'_H,\dot{B}'_H;B_C,\dot{B}_C) \tag{22}$$

On the other hand, the current of H^+ is expected to be given by

$$I = S'_B(B'_H,\dot{B}'_H;A_C,B_C,\dot{B}_C) + R(B'_H,\dot{B}'_H;B_C,\dot{B}_C) \tag{23}$$

Substituting eq 1 and eqs 17−19 into eqs 21−23, we can derive an expression connecting $\Delta I(t)$ with $\Delta P_H(t)$ (Appendix A):

$$\Delta I(t) = K^*_H(\omega)\, \Delta P_H(t) \tag{24}$$

where

$$K^*_H(\omega) \equiv \{k_{PH}k_{AH}(k_{BH} + i\omega l_{BH})/\Theta\} \tag{25}$$

and the short notation

$$\Theta \equiv (k_{-AH} + k_{AH} + i\omega)\{k_{-BH} + k_{BH} + i\omega(1 + l_{-BH} + l_{BH})\} - k_{AH}(k_{-BH} + i\omega l_{-BH}) \tag{26}$$

has been used. The definitions for the seven parameters involved in $K^*_H(\omega)$ are listed in the first row of Table 1; partial derivatives with respect to B and $\dot{B}$ are distinguished by k and l, respectively.

It is noted that A_C and B_C have been fixed in the derivation, because P_C was kept constant in this case.

(2) In a $H_2//\tilde{C}^{2-}$ Case. Let us consider the other case where P_C is perturbed. The appearance rates of A_C and B_C species can be expressed by

$$dA_C/dt = S'_A(P_C,A_C) - S'_B(B'_H,\dot{B}'_H;A_C,B_C,\dot{B}_C) \tag{27}$$

and

$$dB_C/dt = S'_B(B'_H\dot{B}'_H;A_C,B_C,\dot{B}_C) - R(B'_H,\dot{B}'_H;B_C,\dot{B}_C) \tag{28}$$

The current of H^+ may be given again by eq 23.

Substituting eq 1 and eqs 17−19 into eqs 27, 28, and 23, we can derive (Appendix B)

$$\Delta I(t) = K^*_C(\omega)\, \Delta P_C(t) \tag{29}$$

where

$$K^*_C(\omega) \equiv k_{PC}k_{AC}\{2k_{BC} + i\omega(1 + 2l_{BC})\}/\Phi \tag{30}$$

TABLE 2: Experimental Conditions and Parameters Evaluated by Computer Simulation (X: H or C)

				X →	← A →		← B →		← $\dot{B}$ →		
	catal.	E_C[a] (mV)	$\lvert I_C\rvert$ (mA)	k_{PX} (mA/Torr)	k_{-AX} (min^{-1})	k_{AX}	k_{-BX} (min^{-1})	k_{BX}	l_{-BX}	l_{BX}	mean dev. $\delta^b \times 10^2$
ΔP_H	Pt//Pt	21.8	1.15	7.89	279	5.9	7.5	4.60	0.00	1.00	2.31
	Pt′//Pt′	−22.7	1.85	9.11	133	0.90	0.95	42.6	0.09	0.92	2.21
	Rh//Rh	−5.0	0.64	3.03	59.8	0.35	1.69	16.1	0.94	0.00	3.56
ΔP_C	Pt//Pt	−61	1.22	0.024	4.8	7.9	18.6	11.8	-0.16_3	-0.83_3	3.99
	Pt′//Pt′	−5.0	3.26	0.023	21.0	9.86	7.76	9.80	−0.13	−0.85	5.06
	Rh//Rh	22.5	0.62	0.024	0.14	0.66	0.54	0.10	−0.17	−0.78	4.02

[a] The negative value of E_C means that the current $|I_c|$ was hindered by the supplied voltage. [b] $\delta \equiv (1/N)\Sigma_N[\{K^*_{obs}(\omega) - K^*_X(\omega)\}^2]^{1/2}/(\Delta I_\omega/\Delta P)_{max}$, where N denotes the number of data and $(\Delta I_\omega/\Delta P)_{max}$ is the maximum value of $(\Delta I_\omega/\Delta P)$ obtained in each run.

and the short notation

$$\Phi \equiv (k_{-AC} + k_{AC} + i\omega)\{k_{-BC} + k_{BC} + i\omega(1 + l_{-BC} + l_{BC})\} - k_{AC}(k_{-BC} + i\omega l_{-BC}) \quad (31)$$

has been used. The definitions for the seven parameters involved in $K^*_C(\omega)$ are listed in the second row of Table 1.

5. Data Analysis

5.1. FR to $\Delta P_H(t)$. Comparing the real and imaginary parts of $K^*_{obs}(\omega)$ in eq 4 with those of $K^*_H(\omega)$ in eq 25, we get two relations:

$$\mathrm{Re}\{K^*_H(\omega)\} = (\Delta I_\omega/\Delta P_H)\cos\phi \quad (32)$$

and

$$-\mathrm{Im}\{K^*_H(\omega)\} = (\Delta I_\omega/\Delta P_H)\sin\phi \quad (33)$$

Matching the calculated results on the left-hand side of eqs 32 and 33 to the experimental ones on the right-hand side plotted in Figure 8a, we evaluated the seven parameters involved in $K^*_H(\omega)$ by computer simulation on a trial and error basis. The calculated results are shown by the small circles in Figure 8a, and the parameters concluded are summarized in Table 2. Evidently the calculated results can also lead to $(\Delta I_\omega/\Delta P_H)_{calc}$ and ϕ_{calc} individually; the results are demonstrated as a function of ω by the solid curves in Figure 6a,b. Since the experimental errors were within the size of each symbol, we can say that they were reproduced well by $K^*_H(\omega)$.

5.2. FR to $\Delta P_C(t)$. Comparing $K^*_{obs}(\omega)$ in eq 4 with $K^*_C(\omega)$ in eq 30, we get two relations:

$$\mathrm{Re}\{K^*_C(\omega)\} = (\Delta I_\omega/\Delta P_C)\cos\phi \quad (34)$$

and

$$-\mathrm{Im}\{K^*_C(\omega)\} = (\Delta I_\omega/\Delta P_C)\sin\phi \quad (35)$$

Matching the calculated results on the left-hand side of eqs 34 and 35 to the experimental ones on the right-hand side plotted in Figure 8b, we evaluated the seven parameters involved in $K^*_C(\omega)$ by computer simulation on a trial and error basis. The calculated results are shown by the small circles in Figure 8b, and the parameters concluded are given in Table 2. The calculated results can also lead to $(\Delta I_\omega/\Delta P_C)_{calc}$ and ϕ_{calc}; the results are demonstrated as a function of ω by the solid curves in Figures 7a,b. They also agreed well with the measurements within experimental error.

6. Discussion

If all l's in $K^*_H(\omega)$ and $K^*_C(\omega)$ are fixed at zero, these functions are reduced to characteristic functions derived from ordinary rate equations (excluding the additional variable $\dot{B}$), $K^*_{Hm}(\omega)$ and $K^*_{Cm}(\omega)$:

$$K^*_{Hm}(\omega) = k_{PH}k_{AH}k_{BH}/\Theta_m \quad (36)$$

where

$$\Theta_m \equiv (k_{-AH} + k_{AH} + i\omega)(k_{-BH} + k_{BH} + i\omega) - k_{AH}k_{-BH} \quad (37)$$

and

$$K^*_{Cm}(\omega) = k_{PC}k_{AC}(2k_{BC} + i\omega)/\Phi_m \quad (38)$$

where

$$\Phi_m \equiv (k_{-AC} + k_{AC} + i\omega)(k_{-BC} + k_{BC} + i\omega) - k_{AC}k_{-BC} \quad (39)$$

Since $K^*_{Hm}(\omega)$ is always above the x-axis and usually intersects the y-axis in Figure 8a, it is evidently impossible to explain the various FR data demonstrated in Figure 8a. Further, since $K^*_{Cm}(\omega)$ is usually asymptotic to (0, 0) as $\omega \to \infty$ along the y-axis from the upper side in Figure 8b, all actual data cannot be interpreted by $K^*_{Cm}(\omega)$. However, $K^*_C(\omega)$ becomes asymptotic to (0, 0) from the lower side if $1 + 2l_{BC} < 0$ or $l_{BC} < -0.5$ is satisfied (see Table 2).

Although the physical meaning remains obscure, the working hypothesis of $\dot{B}$ was effective in the data analysis. To confirm its validity, a variety of conclusions that can be derived from the evaluated parameters in Table 2 will be discussed below.

6.1. Ordinary Rate Constant, *k*. (1) The two rate constants concerned with S_A at the first stage of H_2 are defined as

$$k_{PH} \equiv (\partial S_A/\partial P_H)_A \quad (40)$$

and

$$k_{-AH} \equiv -(\partial S_A/\partial A_H)_P \quad (41)$$

Although k_{PH} in eq 40 depends on the amount of catalysts, k_{-AH} is independent of the amount of catalysts, because both numerator S_A and denominator A_H depend in the same way on the amount of catalysts; the other three k's in Table 1 or 2, k_{AH}, k_{-BH}, and k_{BH}, are also independent of the amount of catalysts. This is a great advantage of the present FR method because they are characteristic of active sites and therefore can be compared with each other.

On the basis of the values for k_{PH}'s and k_{PC}'s in Table 2, it is concluded that (i) adsorption of H_2 is faster than $C_3{}^{2-}$ over both catalysts because

$$k_{PH} \gg k_{PC} \qquad \text{over both catalysts} \quad (42)$$

(ii) both reverse and forward rates of A_X species over Pt are faster than those over Rh because

$$k_{-\mathrm{AX}}\text{ over Pt} > k_{-\mathrm{AX}}\text{ over Rh}$$

$$k_{\mathrm{AX}}\text{ over Pt} > k_{\mathrm{AX}}\text{ over Rh (X: H and C)} \tag{43}$$

(2) The rate constant k_{AH} is defined by

$$k_{\mathrm{AH}} \equiv (\partial S_{\mathrm{B}}/\partial A_{\mathrm{H}})_{\mathrm{B}} \tag{44}$$

Since both $k_{-\mathrm{AH}}$ and k_{AH} are concerned with the same $\mathrm{A_H}$ species, the ratio η_{AH} defined by

$$\eta_{\mathrm{AH}} \equiv k_{\mathrm{AH}}/(k_{-\mathrm{AH}} + k_{\mathrm{AH}}) \tag{45}$$

gives the transition probability of $\mathrm{A_H}$ species to $\mathrm{B_H}$ species.

On the other hand, since $k_{-\mathrm{BH}}$ and k_{BH} are defined as

$$k_{-\mathrm{BH}} \equiv -(\partial S_{\mathrm{B}}/\partial B_{\mathrm{H}})_{\mathrm{A}} \tag{46}$$

and

$$k_{\mathrm{BH}} \equiv [\partial(S'_{\mathrm{B}} + R)/\partial B_{\mathrm{H}}] \tag{47}$$

the ratio η_{BH} defined by

$$\eta_{\mathrm{BH}} \equiv k_{\mathrm{BH}}/(k_{-\mathrm{BH}} + k_{\mathrm{BH}}) \tag{48}$$

gives the transition probability of $\mathrm{B_H}$ species to the half-hydrogenated species and propane.

The values of η_{AH} and η_{BH} and also those of η_{AC} and η_{BC} calculated from k's in Table 2 are summarized in Table 3. It is concluded therefore that (i) most $\mathrm{A_H}$ species reverse to the gas phase over both catalysts because

$$\eta_{\mathrm{AH}} \ll 1 \qquad \text{over both catalysts} \tag{49}$$

while the possibilities for the reverse and forward reactions of both $\mathrm{A_C}$ and $\mathrm{B_C}$ species are comparable over both catalysts because

$$\eta_{\mathrm{AC}}\text{ and }\eta_{\mathrm{BC}} \sim 1/2 \qquad \text{over both catalysts} \tag{50}$$

(ii) the transition probability of $\mathrm{B_C}$ species to propane over Pt is greater than that over Rh because

$$\eta_{\mathrm{BC}}\text{ over Pt} > \eta_{\mathrm{BC}}\text{ over Rh} \tag{51}$$

(3) Since the sum of $k_{-\mathrm{AH}} + k_{\mathrm{AH}}$ gives the (whole) rate constant for the disappearance of $\mathrm{A_H}$ species, provided that each rate is proportional to $\mathrm{A_H}$, the inverse is expected to give a mean residence time of the adsorbed species, τ_{AH}:

$$\tau_{\mathrm{AH}} = 1/(k_{-\mathrm{AH}} + k_{\mathrm{AH}}) \tag{52}$$

In the same way, the mean residence time of $\mathrm{B_H}$ species, τ_{BH}, could be given by

$$\tau_{\mathrm{BH}} = 1/(k_{-\mathrm{BH}} + k_{\mathrm{BH}}) \tag{53}$$

The results calculated from the values in Table 2 are compared in Table 4. It is concluded therefore that (i) the residence time of $\mathrm{A_H}$ species is shorter than that of $\mathrm{B_H}$ species over both catalysts because

$$\tau_{\mathrm{AH}} < \tau_{\mathrm{BH}} \qquad \text{over both catalysts} \tag{54}$$

(ii) the residence time of $\mathrm{A_H}$ species is shorter than that of $\mathrm{A_C}$ species over both catalysts because

$$\tau_{\mathrm{AH}} < \tau_{\mathrm{AC}} \qquad \text{over both catalysts} \tag{55}$$

TABLE 3: Transition Probability of $\mathrm{A_X}$ Species to $\mathrm{B_X}$ Species ($=\eta_{\mathrm{AX}}$) and That of $\mathrm{B_X}$ Species to Product(s) ($=\eta_{\mathrm{BX}}$) (X: H or C)

catal.	η_{AH}[a]	η_{BH}[b]	η_{AC}[a]	η_{BC}[b]
Pt//Pt	0.021	0.38	0.62	0.39
Pt'//Pt'	0.007	0.98	0.32	0.56
Rh//Rh	0.006	0.91	0.83	0.16

[a] $\eta_{\mathrm{AX}} = k_{\mathrm{AX}}/(k_{-\mathrm{AX}} + k_{\mathrm{AX}})$. [b] $\eta_{\mathrm{BX}} = k_{\mathrm{BX}}/(k_{-\mathrm{BX}} + k_{\mathrm{BX}})$.

TABLE 4: Mean Residence Times of $\mathrm{A_X}$- and $\mathrm{B_X}$ Species (X: H or C)

catal.	τ_{AH}/s[a]	τ_{BH}/s[b]	τ_{AC}/s[a]	τ_{BC}/s[b]
Pt//Pt	0.21	5.0	4.7	2.0
Pt'//Pt'	0.45	1.4	1.9	3.4
Rh//Rh	1.0	3.4	75	94

[a] $\tau_{\mathrm{AX}} = 1/(k_{-\mathrm{AX}} + k_{\mathrm{AX}})$. [b] $\tau_{\mathrm{BX}} = 1/(k_{-\mathrm{BX}} + k_{\mathrm{BX}})$.

(iii) the residence time of $\mathrm{A_C}$ species over Pt is considerably shorter than that over Rh because

$$\tau_{\mathrm{AC}}\text{ over Pt} \ll \tau_{\mathrm{AC}}\text{ over Rh} \tag{56}$$

(iv) the residence time of $\mathrm{B_C}$ species over Pt is considerably shorter than that over Rh because

$$\tau_{\mathrm{BC}}\text{ over Pt} \ll \tau_{\mathrm{BC}}\text{ over Rh} \tag{57}$$

6.2. Novel Rate Constant, *l*. (1) The two novel rate constants concerning $\mathrm{B_H}$ species are defined by

$$l_{-\mathrm{BH}} \equiv -(\partial S_{\mathrm{B}}/\partial \dot{B}_{\mathrm{H}}) \tag{58}$$

and

$$l_{\mathrm{BH}} \equiv [\partial(S'_{\mathrm{B}} + R)/\partial \dot{B}_{\mathrm{H}}] \tag{59}$$

It is worth noting that these constants are nondimensional. On the other hand, those concerning $\mathrm{B_C}$ species are given by

$$l_{-\mathrm{BC}} \equiv -(\partial S'_{\mathrm{B}}/\partial \dot{B}_{\mathrm{C}}) \tag{60}$$

and

$$l_{\mathrm{BC}} \equiv (\partial R/\partial \dot{B}_{\mathrm{C}}) \tag{61}$$

The results in Table 2 show that (i) the novel rate constant concerning hydrogen is positive over both catalysts,

$$l_{-\mathrm{BH}}\text{ and }l_{\mathrm{BH}} > 0 \qquad \text{over both catalysts} \tag{62}$$

whereas the constant concerning propylene is negative over both catalysts,

$$l_{-\mathrm{BC}}\text{ and }l_{\mathrm{BC}} < 0 \qquad \text{over both catalysts} \tag{63}$$

(ii) A remarkable difference between Pt and Rh was derived in l's,

$$l_{\mathrm{BH}} \approx 1 \qquad \text{over Pt} \tag{64}$$

whereas

$$l_{-\mathrm{BH}} \approx 1 \qquad \text{over Rh} \tag{65}$$

(2) Numerous investigators have employed steady-state kinetic measurements in catalytic hydrogenation of light olefins and concluded that when the overall rate R_0 was expressed by

$$R_0 = kP_{\mathrm{H}}^{m}P_{\mathrm{C}}^{n}$$

TABLE 5: Elapsed Times for the Reverse and Forward Reactions of B_C Species

catal.	$\bar{t}_{-BC}$/s[a]	$\bar{t}_{BC}$/s[b]
Pt//Pt	0.53	4.2
Pt′//Pt′	1.0	5.2
Rh//Rh	18.9	468

[a] $\bar{t}_{-BC} = -l_{-BC}/k_{-BC}$. [b] $\bar{t}_{BC} = -l_{BC}/k_{BC}$.

the orders of reaction, m and n, were[7,8,12]

$$m \approx 1 \text{ and } n \leq 0$$

The opposite signs in l's concerned with hydrogen and propylene suggest that if a reactant plays an active role, the value of l concerning the reactant becomes positive, while if a reactant plays a passive role, l of the reactant becomes negative.

6.3. Complex Rate Constant, $k + i\omega l$. Each novel rate equation involving B and $\dot{B}$ leads to a "complex rate constant" (more strictly, coefficient); for example, eq 15 leads to

$$\Delta R(t) = (k'_{BH} + i\omega l'_{BH})\Delta B_H(t) \tag{66}$$

or

$$\Delta R(t) = (k_{BC} + i\omega l_{BC})\Delta B_C(t) \tag{67}$$

provided that either P_H or P_C is varied, respectively.

The negative values of $l(-l \equiv l' > 0)$ in eq 63 could be interpreted as follows: the complex rate constant in eq 67 can be transformed as

$$k - i\omega l' \approx k \exp(-i\omega l'/k) \tag{68}$$

in a lower ω region where $\omega \ll k/l'$ is satisfied. Substituting eq 68 into eq 67, we have

$$\Delta R(t) = k_{BC}\Delta B_C(t - \bar{t}_{BC}), \quad \bar{t} \equiv l'/k_{BC} \tag{69}$$

Therefore, l'/k can be regarded as a time lag or an elapsed time, $\bar{t}$, at the elementary step. The results calculated from the values in Table 2 are summarized in Table 5.

6.4. Extreme Case of $\omega \to 0$. (1) Let us consider the steady state corresponding to $\omega \to 0$. According to the results given in Appendices A and B, we have

$$\lim_{\omega \to 0} \Delta A^*_{\omega,H} = \{k_{PH}(k_{-BH} + k_{BH})/\Theta_0\}\Delta P_H \tag{70}$$

and

$$\lim_{\omega \to 0} \Delta B^*_{\omega,H} = \{k_{PH}k_{AH}/\Theta_0\}\Delta P_H \tag{71}$$

where

$$\Theta_0 \equiv (k_{-AH} + k_{AH})(k_{-BH} + k_{BH}) - k_{AH}k_{-BH} \tag{72}$$

Evidently, the gradient of the adsorption isotherm expressed by $\bar{A}_H(\bar{P}_H)$ or $\bar{B}_H(\bar{P}_H)$ can be given by the coefficient in parentheses in eq 70 or 71, respectively.

Further, dividing eq 71 by eq 70, we have the ratio of the two gradients of their adsorption isotherms:

$$\frac{(d\bar{B}_H/d\bar{P}_H)}{(d\bar{A}_H/d\bar{P}_H)}\left(\equiv \frac{\bar{K}_{BH}}{\bar{K}_{AH}}\right) = \lim_{\omega \to 0} \frac{\Delta B^*_{\omega,H}}{\Delta A^*_{\omega,H}} = \frac{k_{AH}}{k_{-BH} + k_{BH}} \tag{73}$$

In the same way, we can obtain the following relations:

$$\lim_{\omega \to 0} \Delta A^*_{\omega,C} = \{k_{PC}(k_{-BC} + k_{BC})/\Phi_0\}\Delta P_C \tag{74}$$

$$\lim_{\omega \to 0} \Delta B^*_{\omega,C} = \{k_{PC}k_{AC}/\Phi_0\}\Delta P_C \tag{75}$$

where

$$\Phi_0 \equiv (k_{-AC} + k_{AC})(k_{-BC} + k_{BC}) - k_{AC}k_{-BC} \tag{76}$$

Therefore, we have the ratio of the gradients of their adsorption isotherms:

$$\frac{(d\bar{B}_C/d\bar{P}_C)}{(d\bar{A}_C/d\bar{P}_C)}\left(\equiv \frac{\bar{K}_{BC}}{\bar{K}_{AC}}\right) = \lim_{\omega \to 0} \frac{\Delta B^*_{\omega,C}}{\Delta A^*_{\omega,C}} = \frac{k_{AC}}{k_{-BC} + k_{BC}} \tag{77}$$

The results calculated from the values in Table 2 are given in Table 6. It is concluded therefore that (i) the gradient of the adsorption isotherm of B_H species, $\bar{K}_{BH}$, is considerably smaller than that of A_H species, $\bar{K}_{AH}$, over both catalysts because

$$\bar{K}_{BH}/\bar{K}_{AH} < 1 \qquad \text{over both catalysts} \tag{78}$$

(ii) the gradient of the adsorption isotherm of B_C species, $\bar{K}_{BC}$, is smaller than that of A_C species, $\bar{K}_{AC}$, over both catalysts because

$$\bar{K}_{BC}/\bar{K}_{AC} \leq 1 \qquad \text{over both catalysts} \tag{79}$$

(2) Since all rate equations ought to agree in a steady state with the overall reaction rate R_0, we have

$$\begin{aligned} R_0 &= S_A(\bar{P}_H,\bar{A}_H) = S_B(\bar{A}_H,\bar{B}_H,0) = S'_A(\bar{P}_C,\bar{A}_C) \\ &= S'_B(\bar{B}'_H,0;\bar{A}_C,\bar{B}_C,0) = R(\bar{B}'_H,0;\bar{B}_C,0) \end{aligned} \tag{80}$$

In traditional methods based on steady-state kinetic studies, dependence of R_0 on $\bar{P}$, $\bar{A}$, and/or $\bar{B}$ has been discussed. The overall rate at a stage was often divided into two parts, corresponding to the forward and reverse reaction rates; for example,

$$S_A(\bar{P}_H,\bar{A}_H) = v_{+A} - v_{-A}$$

On the basis of deuterium tracing measurements, v_+ and v_- were discussed in detail;[8,13] further, S_A was postulated in a case to be expressed by Langmuirian kinetics.[9]

However, it should be emphasized that (i) any hypothesis has been avoided to rate equations in this work. (ii) k does not correspond to v_+ or v_- but to each derivative such as $(\partial v_+/\partial \bar{P}_H)$ or $-(\partial v_-/\partial \bar{A}_H)$. Therefore, k would only indirectly depend on $\bar{P}$ and $\bar{A}$. (iii) Although the ratio of v_-/v_+ at an elementary step has often been discussed,[8,13] η is concerned with either A or B species.

6.5. Miscellaneous. (1) One experimental point plotted in Figure 8 leads to two simultaneous equations given in eqs 32 and 33 or in eqs 34 and 35; the seven parameters for the H_2|Pt//Pt|$C_3{}^{2-}$ system in the first row in Table 2, for example, were determined by optimizing 20(=10 × 2) simultaneous equations.

(2) Since every experimental datum involves experimental errors, there was an apparent (local) minimum in the computer simulation. Therefore, to decide which minimum is preferable, we considered that the inequality of $\tau_A < \tau_B$ should be satisfied.

(3) The FR spectra obtained with different Pt catalysts were considerably different, as shown in Figure 8, but the origin remained obscure; the differences in k's with respect to hydrogen were greater than those with respect to propylene, while the values of l's were almost identical. The most remarkable difference was in the values of k_{BH}.

TABLE 6: Ratio of the Gradient of the Adsorption Isotherm of B_X Species ($=\bar{K}_{BX}$) to That of the Adsorption Isotherm of A_X Species ($=\bar{K}_{AX}$)

catal.	$\bar{K}_{BH}/\bar{K}_{AH}$[a]	$\bar{K}_{BC}/\bar{K}_{AC}$[b]
Pt//Pt	0.49	0.26
Pt′//Pt′	0.021	0.56
Rh//Rh	0.020	1.03

[a] $\bar{K}_{BH}/\bar{K}_{AH} = k_{AH}/(k_{-BH} + k_{BH})$. [b] $\bar{K}_{BC}/\bar{K}_{AC} = k_{AC}/(k_{-BC} + k_{BC})$.

(4) Dependence of the rate constants on E_C and/or I_C (see Table 2) remained obscure.

Both mass and energy must be conserved at every elementary step although their separation is difficult, while energy conservation law usually plays an important role in mechanical kinetics. It seems of interest that "adsorption-assisted desorption" has been observed by Yamada et al.,[14,15] suggesting a role of $\dot{B}$. A possible explanation for the role is as follows: since the reaction is exothermic, the temperature at active sites would necessarily be higher than surroundings and would be affected by $\dot{B}$ rather than $\dot{A}$. The opposite signs in l's with respect to ΔP_H and ΔP_C suggest heat effects.

7. Concluding Remarks

One can often obtain a wide variety of models that account for observed kinetic phenomena. However, it should be emphasized that (i) if the kinetic model demonstrated in Figure 10 is accepted, both K^*_H and K^*_C may be derived straightforwardly on the basis of material balance only, although the following two relations are essential: $\Delta B'_H = g\Delta B_H$ in eq 16 and $\Delta I = \Delta S'_B + \Delta R$ from eq 23. (ii) The various FR spectra in Figure 8a,b covering a wide range of ϕ, $140° > \phi > -6°$ for ΔP_H and $260° > \phi > 23°$ for ΔP_C, have been reproduced well by K^*_H and K^*_C, which are very flexible due to the novel rate constant l. (iii) Various conclusions that were derived from the evaluated parameters appear to be reasonable; at least, they contain no conflicts such as $k < 0$ and $|l| > 1$.

It is worth noting that (iv) the rate constants concerning the reverse reaction as well as the forward one have been derived from the FR spectrum without any isotope-tracing measurements.

Although the ability of their kinetic model to describe the experimentally observed FR spectra cannot be considered as a final proof for the validity of the suggested model, the present results do point to the efficiency of the present FR method. To verify the working hypothesis of $\dot{B}$, we evidently need more measurements with other combinations of metals and/or reactants.

Appendix A

Substituting eq 1 and eqs 17−19 into eq 21, we have

$$i\omega\Delta A^*_{\omega,H} = (k_{PH}\Delta P_H - k_{-AH}\Delta A^*_{\omega,H}) - (k_{AH}\Delta A^*_{\omega,H} - k_{-BH}\Delta B^*_{\omega,H} - i\omega l_{-BH}\Delta B^*_{\omega,H}) \quad \text{(A-1)}$$

which may be rewritten as

$$(k_{-AH} + k_{AH} + i\omega)\Delta A^*_{\omega,H} = k_{PH}\Delta P_H + (k_{-BH} + i\omega l_{-BH})\Delta B^*_{\omega,H} \quad \text{(A-2)}$$

On the other hand, substituting eq 1 and eqs 17−19 into eq 22, we have after some rearrangements

$$\{k_{-BH} + k_{BH} + i\omega(1 + l_{-BH} + l_{BH})\}\Delta B^*_{\omega,H} = k_{AH}\Delta A^*_{\omega,H} \quad \text{(A-3)}$$

In the derivation, A_C and B_C have been regarded as constant, because $\Delta P_C(t) = 0$ in this case. Since direct proportion between B′$_H$ and B$_H$ species is assumed, we have

$$B'_H = gB_H \ (g\text{: constant}) \quad \text{(A-4)}$$

which leads to

$$\left\{\frac{\partial(S'_B + R)}{\partial B'_H}\right\}\Delta B'^*_{\omega,H} = \left\{\frac{\partial(S'_B + R)}{\partial B_H}\right\}\Delta B^*_{\omega,H} = k_{BH}\Delta B^*_{\omega,H} \quad \text{(A-5)}$$

This relation has been used in the derivation of eq A-3.

Combining eqs A-2 and A-3, we have

$$\Delta A^*_{\omega,H} = k_{PH}\{k_{-BH} + k_{BH} + i\omega(1 + l_{-BH} + l_{BH})\}\Delta P_H/\Theta \quad \text{(A-6)}$$

and

$$\Delta B^*_{\omega,H} = k_{PH}k_{AH}\Delta P_H/\Theta \quad \text{(A-7)}$$

where

$$\Theta \equiv (k_{-AH} + k_{AH} + i\omega)\{k_{-BH} + k_{BH} + i\omega(1 + l_{-BH} + l_{BH})\} - k_{AH}(k_{-BH} + i\omega l_{-BH}) \quad \text{(A-8)}$$

On the other hand, eq 23 leads to the variation in the current of H$^+$ induced by $\Delta P_H(t)$:

$$\Delta I^*_\omega = \left\{\frac{\partial(S'_B + R)}{\partial B'_H}\right\}\Delta B'^*_{\omega,H} + \left\{\frac{\partial(S'_B + R)}{\partial \dot{B}'_H}\right\}i\omega\Delta B'^*_{\omega,H} = (k_{BH} + i\omega l_{BH})\Delta B^*_{\omega,H} \quad \text{(A-9)}$$

Substituting eq A-7 into eq A-9, we have $K^*_H(\omega)$ in eq 25.

Appendix B

Substituting eq 1 and eqs 17−19 into eqs 27 and 28, we have after some rearrangements

$$(k_{-AC} + k_{AC} + i\omega)\Delta A^*_{\omega,C} = k_{PC}\Delta P_C + (k_{-BC} + i\omega l_{-BC})\Delta B^*_{\omega,C} \quad \text{(B-1)}$$

and

$$\{k_{-BC} + k_{BC} + i\omega(1 + l_{-BC} + l_{BC})\}\Delta B^*_{\omega,C} = k_{AC}\Delta A^*_{\omega,C} \quad \text{(B-2)}$$

where A_H and B_H have been regarded as constant, because $\Delta P_H(t) = 0$ in this case.

Combining eqs B-1 and B-2, we have

$$\Delta A^*_{\omega,C} = k_{PC}\{k_{-BC} + k_{BC} + i\omega(1 + l_{-BC} + l_{BC})\}\Delta P_C/\Phi \quad \text{(B-3)}$$

and

$$\Delta B^*_{\omega,C} = k_{PC}k_{AC}\Delta P_C/\Phi \quad \text{(B-4)}$$

where

$$\Phi \equiv (k_{-AC} + k_{AC} + i\omega)\{k_{-BC} + k_{BC} + i\omega(1 + l_{-BC} + l_{BC})\} - k_{AC}(k_{-BC} + i\omega l_{-BC}) \quad \text{(B-5)}$$

On the other hand, eq 23 leads to the variation in the current of H$^+$ induced by $\Delta P_C(t)$:

$$\Delta I^*_{\omega} = k_{\mathrm{AC}}\Delta A^*_{\omega,\mathrm{C}} - (k_{-\mathrm{BC}} + \mathrm{i}\omega l_{-\mathrm{BC}})\Delta B^*_{\omega,\mathrm{C}} + (k_{\mathrm{BC}} + \mathrm{i}\omega l_{\mathrm{BC}})\Delta B^*_{\omega,\mathrm{C}} \quad \text{(B-6)}$$

Substituting eqs B-3 and B-4 into eq B-6, we have $K^*_{\mathrm{C}}(\omega)$ in eq 30.

References and Notes

(1) Bernasconi, C. F. *Relaxation Kinetics*; Academic Press: New York, 1976.

(2) Eigen, M.; DeMaeyer, L. *Techniques of Organic Chemistry*; Friess, S. L., Lewis, E. S., Weissberger, A., Eds.; Interscience: New York, 1963; Vol. 8, Part 2, p 895.

(3) Yasuda, Y. *Heterogen. Chem. Rev.* **1994**, *1*, 103.

(4) Yasuda, Y. *J. Phys. Chem.* **1989**, *93*, 7185.

(5) Takenaka, H.; Torikai, E. *Jpn. Kokai Tokkyo Koho* **1980**, *55*, 38934.

(6) Polanyi, M.; Horiuti, J. *Trans. Faraday Soc.* **1934**, *30*, 1164.

(7) Bond, G. C. *Catalysis by Metals*; Academic Press: London, 1962.

(8) Horiuti, J.; Miyahara, K. *Hydrogenation of Ethylene on Metallic Catalysts*; NBS-NSRDS No. 13; Government Printing Office: Washington, DC, 1968.

(9) Rekoske, J. E.; Cortright, R. D.; Goddard, S. A.; Sharma, S. B.; Dumesic, J. A. *J. Phys. Chem.* **1992**, *96*, 1880.

(10) Yasuda, Y.; Nomura, K. *J. Phys. Chem.* **1993**, *97*, 3319.

(11) Yasuda, Y. *Studies in Surface Science and Catalysis*; Weitkamp, J., Karge, H. G., Pfeifer, H., Hölderich, W., Eds.; (1994 Elsevier Science B. V.: Amsterdam, 1994; Vol. 84, p 1331.

(12) Mann, R. S.; Lien, T. R. *J. Catal.* **1969**, *15*, 1.

(13) Sato, S.; Iyama, T.; Miyahara, K. *J. Catal.* **1981**, *69*, 77.

(14) Yamada, T.; Onishi, T.; Tamaru, K. *Surf. Sci.* **1983**, *133*, 533.

(15) Yamada, T.; Tamaru, K. *Surf. Sci.* **1984**, *146*, 341.

JP950732R